The Temperature Sensitivity of Miniature Endplate Currents Is Mostly Governed by Channel Gating: Evidence from Optimized Recordings and Monte Carlo Simulations

Joel R. Stiles*, Irina V. Kovyazina*§, Edwin E. Salpeter# and Miriam M. Salpeter*
*Section of Neurobiology and Behavior, and #Departments of Physics and Astronomy, Cornell University, Ithaca, New York 14853-2702, and §Kazan Institute of Biochemistry and Biophysics of Russian Academy of Sciences, Kazan 420503 Box 30, Russia

ABSTRACT The temperature dependence of miniature endplate current (MEPC) amplitude (A_c), 20–80% rise time (t_r), and 90–33% fall-time (t_f) was determined for lizard (*Anolis carolinensis*) intercostal muscle using broadband extracellular (EC) and voltage clamp (VC) recordings. Voltage clamp methods were optimized for the fast MEPC rising phase using custom electronics. From 0–43°C, A_c increased by ~4.2-fold, while t_r and t_f decreased by ~3.6- and ~9.5-fold, respectively. Arrhenius plots were smoothly curved, with small apparent Q_{10} (A_c) or $(Q_{10})^{-1}$ (t_r and t_f) values mostly well below 2.0. Nearly identical extracellular and voltage clamp results ruled out measurement artifacts, even for the shortest t_r values (<60 μs). Monte Carlo simulation of MEPCs showed that a single underlying rate cannot determine the observed temperature dependence. To quantitatively reproduce the experimental t_f results, a minimal model required activation energies of 46.0 ($Q_{10} \sim 2.0$) and 63.6 ($Q_{10} \sim 2.5$) kJ mol^{-1} for channel opening and closing, respectively, and accounted for most of the observed changes in A_c and t_r as well. Thus, relatively large but offsetting temperature sensitivities of channel gating mostly govern and minimize the temperature dependence of MEPCs, preserving the safety factor for neuromuscular transmission. Additional temperature-sensitive parameters that could fine-tune the minimal model are discussed.

INTRODUCTION

The influence of temperature on synaptic current size and time course can provide valuable information about underlying processes such as neurotransmitter diffusion and receptor activation. The temperature dependence of miniature endplate currents (MEPCs) at the adult vertebrate neuromuscular junction has been studied over many years for a variety of muscles and animal species, often with radically different results (e.g., Magleby and Stevens, 1972b; Gage and McBurney, 1975; Dwyer, 1981; Head, 1983; Robertson and Wann, 1984; Harper et al., 1989; Tiiska and Lagerspetz, 1994; Tanzi and D'Angelo, 1995; Van der Kloot, 1995). Given the technical difficulties encountered in measuring fast signals in such large cells, the wide range of literature findings may reflect limited recording accuracy rather than physiological differences. To improve recording accuracy, we recently developed wide bandwidth, optimized voltage clamp (VC) and extracellular (EC) methods to record MEPCs (Stiles et al., 1996). In the present study, we used further optimized methods to re-examine MEPC temperature dependence over a very wide range (0–43°C). Monte Carlo computer simulations (Bartol et al., 1991; Anglister et al., 1994; Stiles et al., 1996; Stiles et al., 1998a) were then used to model MEPC generation and to test different possible mechanisms for the observed temperature dependence.

In principle, at any single temperature, the MEPC amplitude (A_c), rise time (t_r), and *e*-fold fall time (t_f) must depend on the rates of many different processes, including acetylcholine (ACh) release by exocytosis, ACh diffusion within the synaptic cleft, ACh binding to and unbinding from ACh receptor (AChR), AChR channel gating (opening and closing), and ACh hydrolysis by acetylcholinesterase (AChE). Some of these rates depend strongly on temperature, with apparent Q_{10} values of 2–4 (e.g., AChR gating [Sachs and Lecar, 1977; Dilger et al., 1991; Zanello et al., 1996], AChE hydrolysis [Froede and Wilson, 1971; Rosenberry, 1975], exocytotic fusion pore expansion in mast cells [Spruce et al., 1990]), whereas others (e.g., diffusion) are likely to be far less sensitive to temperature, with Q_{10} values close to unity. We have previously shown that large changes in the rate of ACh hydrolysis or exocytosis can have little or no effect on MEPCs (Anglister et al., 1994; Stiles et al., 1996), so it is very unlikely that all rates underlying MEPC generation (even those that are highly sensitive to temperature) contribute significantly to the effective MEPC temperature sensitivity. One extreme hypothesis would be that a single rate predominates over all others in determining the MEPC temperature dependence. In contrast, if two or more rates contribute significantly, their effects could be synergistic or offsetting. In the latter case, the apparent MEPC temperature dependence could be small despite large temperature sensitivities of the underlying rates. To distinguish between these possibilities, we measured MEPC A_c, t_r, and t_f at many different temperatures, and then determined the simplest possible quantitative model of MEPC temperature dependence. This model consisted of only two offsetting temperature-sensitive rates, and our simulation results agreed surprisingly well with our experimental data. The physio-

Received for publication 28 October 1998 and in final form 6 May 1999.
Address reprint requests to Miriam M. Salpeter, Section of Neurobiology and Behavior, W101 Seeley G. Mudd Hall, Cornell University, Ithaca, NY 14853-2702. Tel.: 607-254-4341; Fax: 607-254-4308; E-mail: mms13@cornell.edu.

0006-3495/99/08/1177/11 $2.00

logical implications of the minimal model are discussed, together with additional factors that could fine-tune the model.

MATERIALS AND METHODS

Intercostal muscle preparation

Miniature endplate current recordings were performed on lizard (*Anolis carolinensis*, Carolina Biological Supply Co., Burlington, NC) intercostal muscle fibers, because they have compact endplates that can be directly visualized for electrode positioning. In addition, the AChR site density and distribution are known (Salpeter et al., 1984), and extensive (room temperature) modeling constraints have been obtained in earlier studies (Land et al., 1980, 1981, 1984; Bartol et al., 1991; Bartol, 1991; Anglister et al., 1994; Stiles et al., 1996). The animals were housed under a controlled day–night cycle and were acclimated to an ambient temperature of 26–28°C for at least several days before an experiment. All surgical procedures were performed in accord with an approved Cornell University Animal Care and Use Committee Protocol (A3347-01). Before each experiment, lizards were first killed by decapitation followed by pithing, and then the left and right halves of the ribcage were dissected to expose single layers of muscle fibers. The bathing medium was a reptile Ringer's solution, pH 7.4 (Land et al., 1980). For MEPC recordings at different temperatures (0–43°C), individual unstained endplates were located using Hoffman modulation optics, and the temperature of the microscope stage was controlled using a recirculating ethanol/water solution. Recording temperatures were determined directly from the recording bath. All chemical reagents were obtained from Sigma Chemical Co. (St. Louis, MO).

MEPC recordings

Our optimized methods for VC and EC recordings were similar to those previously described (Stiles et al., 1996). For EC recordings, large blunt microelectrodes with tip diameters of 20–30 μm were filled with Ringer's solution (0.3–0.5 MΩ, −3 dB at $>$ 10 kHz while immersed), and were gently pressed onto the surface of endplates. The extracellular voltage change corresponding to the time course of an MEPC was amplified using a differential ac amplifier (x1000, model 1700, A-M Systems, Everett, WA). The amplifier's high and low pass filter settings were 1 Hz and 20 kHz, respectively (−3 dB, 2-pole Butterworth response). For VC recordings, short-taper intracellular microelectrodes were pulled to resistances of about 1 MΩ (3 M KCl; −3 dB at ~12 kHz), and were used with a custom-made high speed voltage clamp rig (Stiles et al., 1996). One important modification was added to the electronics described previously. A small variable capacitance was added to the current electrode headstage, allowing critical damping of stray capacitances for the actual immersed microelectrodes before impaling cells. Unlike active compensation for stray capacitances (Finkel, 1985), this feature does not add noise and allows extremely high clamp speeds ($\ll$20 μs 20–80% time for a 1-mV step change) and dynamic accuracy in current measurements. Further details are given elsewhere (Stiles et al., 1998b). External high and low pass filtering for the measured clamp current were at ~0.5 Hz and ~9 kHz, respectively (−3 dB, 4-pole Bessel response).

MEPC data analysis

Analysis methods were identical for EC and VC MEPCs. Individual signals were digitized at 50 kHz, and subsequently fitted using a nonlinear least squares method (Stiles et al., 1996) that oversamples (2×) the raw data. Each individual MEPC was fitted twice. In the first pass, the unsmoothed raw data were fitted to obtain values for peak amplitude (A_c), 20–80% rise time (t_r), and 90–33% (e-fold) decay time (t_f). In the second pass, the raw data were first mildly smoothed using a sliding 8-point (160 μs) trapezoidal window. Such a narrow smoothing window slightly prolongs the rising phase symmetrically around the time point at which 50% A_c is reached. The 50% A_c time obtained by fitting the smoothed data then is used to go back and align the raw, unsmoothed data for signal averaging to improve the signal-to-noise ratio. Thus for each endplate (fiber), mean A_c, t_r, and t_f values could be obtained by two methods, either by averaging individual MEPC values, or by fitting the single mean MEPC obtained after aligning and signal-averaging the raw data. Using a clamped model cell and artificial analog MEPCs (Stiles et al., 1996), we have previously determined that the two methods give virtually identical results. Furthermore, the shape of the input signal can be accurately recovered from the noisy recording data, and our recording and filtering conditions allow accurate measurement of mean t_r values as short as 50 μs. In the present study, mean A_c, t_r, and t_f values for each endplate were averaged over multiple cells, so the error ranges reported here predominantly reflect cell-to-cell variability. The shape of signal-averaged EC and VC MEPCs was used for comparison with simulated MEPCs, and the technique introduced here for critical damping of stray capacitances further optimizes agreement between experimental EC and VC determinations of t_r and MEPC shape.

Computer simulations

Monte Carlo computer simulations of MEPC generation were performed using the program MCell, Version 1.21 (Stiles et al., 1998a), on a Digital Equipment Corporation AlphaStation 250 4/266 running Digital UNIX (OSF/1 Version 3.2B) with 160 Mbytes of RAM. Except as otherwise detailed in Modeling Results and Predictions, the design of the model neuromuscular junction and other input parameters were similar to those described previously for 22°C (Anglister et al., 1994; Stiles et al., 1996). Individual simulated MEPCs were fitted to determine A_c, t_r, and t_f values using the same algorithm and methods applied to experimental MEPCs.

EXPERIMENTAL RESULTS

Figure 1 shows typical examples of individual EC and VC MEPCs recorded at three different temperatures (4, 22, and 38°C). For the sake of comparison, the EC traces have been scaled to approximately match the amplitudes of the VC traces (quantitative measurement of MEPC amplitude is only obtained from VC recordings; hence, subsequent analysis of EC data is shown only for the MEPC time course).

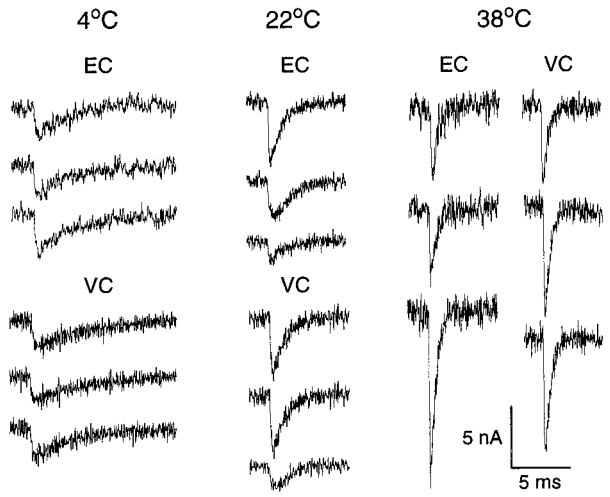

FIGURE 1 Individual MEPC recordings at three different temperatures. Representative examples are shown for different MEPCs recorded either with optimized voltage clamp (VC) or extracellular (EC) methods. The amplitude calibration bar applies only to VC data, and EC traces are scaled to approximately match the size of VC traces (see text). The signal to noise ratio is similar for EC and VC data at each temperature.

Figure 2A shows corresponding mean MEPC traces obtained after signal-averaging (see Methods). Agreement between the averaged EC and VC traces is extremely close at all three temperatures, with minor differences notable only during the falling phase. Because the falling phase is known to depend strongly on membrane potential (e.g., Magleby and Stevens, 1972a; Anderson and Stevens, 1973; Katz and Miledi, 1973; Gage and McBurney, 1975), slightly faster current decay with EC recordings is expected based on the small difference between our holding potential during VC recordings (−100 mV) and the average resting membrane potential during EC recordings (approximately −90 mV). In two experiments we confirmed earlier reports (Kordas, 1972; Gage and McBurney, 1975) that resting membrane potential is relatively independent of temperature (Table 1), ruling out indirect voltage-dependent effects of temperature in our EC results.

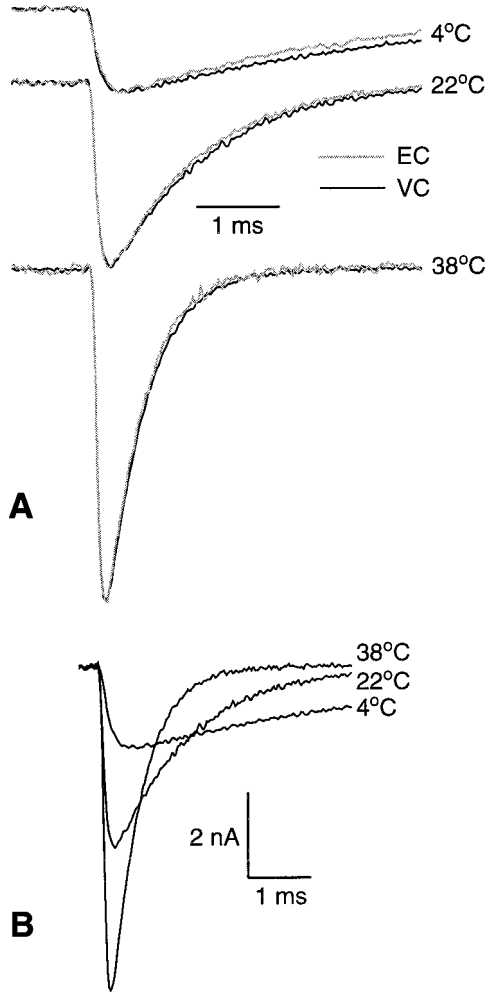

FIGURE 2 Signal-averaged MEPCs at three different temperatures. (*A*) Individual VC and EC MEPCs were aligned and averaged (see Methods; ~100 MEPCs per trace). The resulting waveforms were normalized by amplitude and overlaid for comparison of their shapes. (*B*) Overlay of VC traces from panel A, illustrating relative changes in size and time course as a function of temperature.

TABLE 1 Muscle fiber resting membrane potential varies little with temperature

	Temperature (°C)		
	2.5–5	20–23	37–40
RMP ± SD (mV)	−90 ± 4	−89 ± 4	−97 ± 5
n (muscle fibers)	46	51	46

The three superimposed traces of Fig. 2 *B* are reproductions of the VC traces from Fig. 2 *A*, and exemplify the increased size and faster time course that result with increased temperature. In Table 2, such changes are quantified at four selected temperatures. The A_c, t_r, and t_f values obtained at 21–22°C match our earlier results at 22°C (Stiles et al., 1996), and thus confirm the earlier conclusion that t_r is extremely short (close to 80 μs) at room temperature in this preparation. At the highest temperature indicated in Table 2 (38–39°C), t_r was less than 60 μs, and the excellent agreement between EC and VC measurements again underscores the accuracy of our recording methods. At all four temperatures, the EC t_f value is similar to but slightly less than the corresponding VC value. This finding is consistent with the expectation discussed above for Fig. 2 *A*, based on EC resting membrane potential versus VC holding potential.

To determine the shape of Arrhenius plots for A_c, t_r, and t_f, we recorded MEPCs at many more temperatures than are shown in Table 2. The results are shown in Fig. 3, and all three plots are smoothly curved rather than linear or discontinuous (e.g., exhibiting a sudden break point at low temperatures). For t_r, the EC and VC results are indistinguishable, and for t_f the very small tendency toward a slightly longer VC value is evident. For each measured parameter, the sets of experimental data points were fitted empirically by nonlinear least squares regression (*smooth curves*), using an exponential function that is quadratic in absolute temperature $\{A_c, t_r, \text{or } t_f = \exp[a(°K)^2 + b(°K) + c]\}$.

TABLE 2 Experimental MEPC measurements at four different temperatures

	Temperature (°C)			
	3–4	11–12	21–22	38–39
Peak amplitude (A_c, nA)*				
VC	1.9 ± 0.3	2.6 ± 0.6	3.8 ± 0.7	5.9 ± 1.3
20–80% Rise time (t_r, μs)				
VC	166 ± 21	129 ± 39	84 ± 11	58 ± 8
EC	162 ± 33	107 ± 13	84 ± 10	53 ± 12
90–33% Fall time (t_f, ms)				
VC	4.5 ± 0.5	2.5 ± 0.2	1.4 ± 0.2	0.7 ± 0.1
EC	3.5 ± 0.7	2.1 ± 0.3	1.3 ± 0.3	0.5 ± 0.1
n (endplates)				
VC	8	15	64	21
EC	10	27	42	13

VC and EC indicate voltage clamp and extracellularly recorded data, respectively. Values are mean ± SD averaged over multiple endplates (see Methods; 40–80 MEPCs per endplate).

*Measured only with voltage clamp recordings (see Experimental Results).

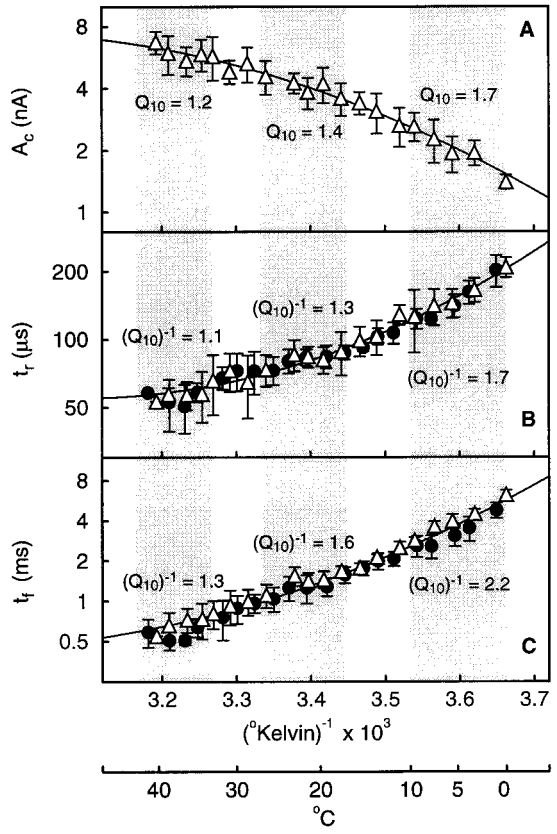

FIGURE 3 Arrhenius plots for experimental (*A*) A_c, (*B*) t_r, and (*C*) t_f determinations. Open triangles and closed circles indicate VC and EC data, respectively (A_c shown only for VC data, as per text and legend for Fig. 1). Note log scaling for ordinate axes. Each point represents the mean ± SD for 5–20 endplates (>200 MEPCs per point). Apparent Q_{10} (A_c, increases with temperature) and $(Q_{10})^{-1}$ (t_r and t_f, decrease with temperature) values were calculated from empirical fitting curves (*solid*) over the 10° intervals indicated by shading.

Using the best fit regression curve for A_c, we calculated three apparent Q_{10} values for three different temperature intervals of 10° (values shown in shaded regions of Fig. 3). For t_r and t_f (which decrease rather than increase with increasing temperature), we calculated corresponding $(Q_{10})^{-1}$ values as indicated. The largest of these values (2.2) was obtained for t_f at low temperatures, and at high temperatures all of the values were very close to unity. These apparent Q_{10} findings are in qualitative agreement with previous less extensive measurements (Dwyer, 1981; Robertson and Wann, 1984; Adams, 1989; Tanzi and D'Angelo, 1995).

MODELING RESULTS AND PREDICTIONS

22°C Input parameter values

Synaptic cleft architecture and ACh release

For computer simulations, we first determined a set of input parameter values that produced simulated MEPCs that matched our experimental MEPCs at 22°C. The AChR and AChE site density and distribution, and primary cleft and junctional fold dimensions, were as previously described for the lizard intercostal muscle preparation (Salpeter et al., 1984; Anglister et al., 1994; Stiles et al., 1996). For most simulations, the release of ACh was modeled as instantaneous appearance of the quantal packet (contained in a volume equal to a synaptic vesicle) in the cleft space above a junctional fold (Bartol et al., 1991; Anglister et al., 1994). We used this simplification because we have previously shown that the results for the MEPC time course are very similar to those obtained if ACh release is modeled explicitly with rapid exocytotic fusion pore expansion (Stiles et al., 1996). In some cases, instantaneous ACh release was not used, and the impact of temperature on ACh exocytosis was modeled using different fusion pore expansion rates. Under these conditions, ACh appeared in the cleft according to the expected time course of vesicle emptying (Stiles et al., 1996; Stiles et al., 1998a).

AChR and AChE reaction mechanisms

For AChR activation, we used the simplest generally accepted kinetic scheme, which we have previously shown is sufficient to closely reproduce the shape of the MEPC rising phase, peak, and falling phase at 22°C (Stiles et al., 1996). This scheme includes two identical, independent ACh binding sites,

$$A + R \underset{k_-}{\overset{2k_+}{\rightleftharpoons}} AR + A \underset{2k_-}{\overset{k_+}{\rightleftharpoons}} A_2R \underset{\alpha}{\overset{\beta}{\rightleftharpoons}} A_2R^*$$

Scheme 1

where A denotes ACh, and R, AR, A_2R, and A_2R* denote the receptor complex in its unbound, singly-bound, doubly-bound closed, and doubly-bound open states, respectively.

For AChE hydrolysis, we used a simplified scheme that ignores unimportant (nonrate-limiting) hydrolytic intermediates,

$$A + AChE \xrightarrow{k_{+E}} A \bullet AChE \xrightarrow{k_{cat}} AChE$$

Scheme 2

where A · AChE is the rate-limiting acetylated enzyme intermediate (Froede and Wilson, 1971; Rosenberry, 1975) that turns over with rate k_{cat}. The mean dwell time of ACh on AChE is thus $1/k_{cat}$.

Input parameter value choices and fitting

With synaptic architecture, AChR and AChE site densities, and ACh release handled as described above, the remaining model inputs include the six rate constants from Schemes 1 and 2 (k_+, k_-, α, β, k_{+E}, and k_{cat}), as well as the number of ACh molecules in a quantal packet (N), the diffusion constant for ACh in the synaptic cleft (D), and the AChR single-channel conductance (γ). Because γ is only a scaling factor that relates simulated MEPC amplitude (number of open channels) to VC current (*nA*), it has no effect on the

MEPC time course, and we simply chose a value (all 22°C input parameter values are summarized in Table 3) reported for garter snake endplate AChR at 22°C (Dionne and Parsons, 1981).

A paper proposing a saturated disk model of MEPC generation (Matthews-Bellinger and Salpeter, 1978) led to a series of experimental and modeling papers (Land et al., 1980, 1981, 1984; Bartol et al., 1991; Stiles et al., 1992, 1996; Anglister et al., 1994). From these, k_{+E} has relatively little impact on the MEPC time course, and we again chose a value consistent with literature estimates (Rosenberry, 1975). We have previously determined k_{cat} for lizard intercostal muscle at room temperature (Table 3), and have shown that MEPC t_f is essentially independent of k_{cat}, k_{+E}, or AChE site density over a very wide range of values (Anglister et al., 1994). Only if the AChE parameter values were extremely small would buffered diffusion (Katz and Miledi, 1973) and late channel openings prolong the falling phase appreciably. Otherwise, t_f is essentially determined by the apparent mean channel open time.

From Scheme 1, each AChR can burst, i.e., open more than once before ACh dissociates, so the apparent mean open time is given by the mean burst duration (MBD), or average elapsed time from the beginning of the first opening to the end of the last opening before dissociation. The mean lifetimes of the A_2R and A_2R^* states are given by $\tau_c = 1/(\beta + 2k_-)$, and $\tau_o = 1/\alpha$, respectively. The mean number of flicker closures ($\overline{nC}$) within a burst of openings is given by $\beta/2k_-$, and by definition, the mean number of openings ($\overline{nO}$) must be one greater than $\overline{nC}$, or $1 + \beta/2k_-$. Hence, MBD is given by,

$$\begin{aligned} \text{MBD} &= (\overline{nO})(\tau_o) + (\overline{nC})(\tau_c) \\ &= (1 + \beta/2k_-)/\alpha + (\beta/2k_-)/(\beta + 2k_-). \end{aligned} \quad (1)$$

From experimental determinations (e.g., Colquhoun and Sakmann, 1985; Dilger et al., 1991), β is much larger than α, and from the modeling studies cited above a value of β/α between 20 and 25 predicts values for other model parameters that are consistent with experimental estimates, and also predicts an MEPC shape that is consistent with our experimental signal-averaged MEPCs. For the present study, we used a midrange value of 22. With $\beta \gg \alpha$, $\tau_c \ll \tau_o$ and the second term in Eq. 1 can be omitted. From this and the near equivalence of t_f and MBD, Eq. 1 can be replaced by the approximate relation,

$$t_f \approx \text{MBD} \approx (1/\alpha) \cdot (1 + \beta/2k_-). \quad (2)$$

From the regression curve in Fig. 3 *C*, t_f at 22°C is 1.25 ms. Also, from the experimental and modeling studies cited above, $\beta/2k_- \approx 1$. Substituting these two values into Eq. 2 gives an initial estimate for α of 1600 s^{-1}, and hence (from $\beta/\alpha = 22$ and $\beta/2k_- \approx 1$) initial values for β and k_- of 35,200 and 17,600 s^{-1}, respectively. From the previous modeling studies cited above, our initial values for D, N, and k_+ were consistent with $\beta/\alpha = 22$, and were 3×10^{-6} cm^2s^{-1}, 6000, and 8×10^7 $M^{-1}s^{-1}$, respectively.

Based on these initial values, we ran multiple (10–20) MCell simulations using different sets of random numbers. The simulated MEPCs (which differ slightly because of stochastic variability, e.g., Fig. 4) then were fitted individually to determine A_c, t_r, and t_f (see Methods). Next, the A_c, t_r, and t_f values were averaged, and the resulting means were compared to the experimental targets (4.15 nA, 79 μs, and 1.25 ms, respectively) obtained from the regression curves of Fig. 3. We then adjusted the input values for α, D, N, and k_+, keeping $\beta = 2k_-$ and $\beta/\alpha = 22$ constant. After several cycles of such adjustments, the simulation A_c, t_r, and t_f values essentially matched our experimental results (see below). For each step of the cycle, adjustments were guided by two approximate scaling relations derived from the saturated disk model: (1) multiplying k_+, k_-, α, β, and D by the same factor (ξ) leaves A_c unchanged but multiplies t_r and t_f by $1/\xi$; and (2) multiplying N and D by the same factor η leaves t_r and t_f unchanged but multiplies A_c by η.

Our final model input values for 22°C are listed in Table 3, and give the following simulation values for A_c, t_r, and t_f (mean ± SD for 10 simulations using different random numbers): 4.12 ± 0.12 nA (749 ± 21 open channels), 84 ±

TABLE 3 Model parameter values at 22°C, and relative sensitivities of simulated MEPC A_c, t_r, and t_f to changes in individual model parameters

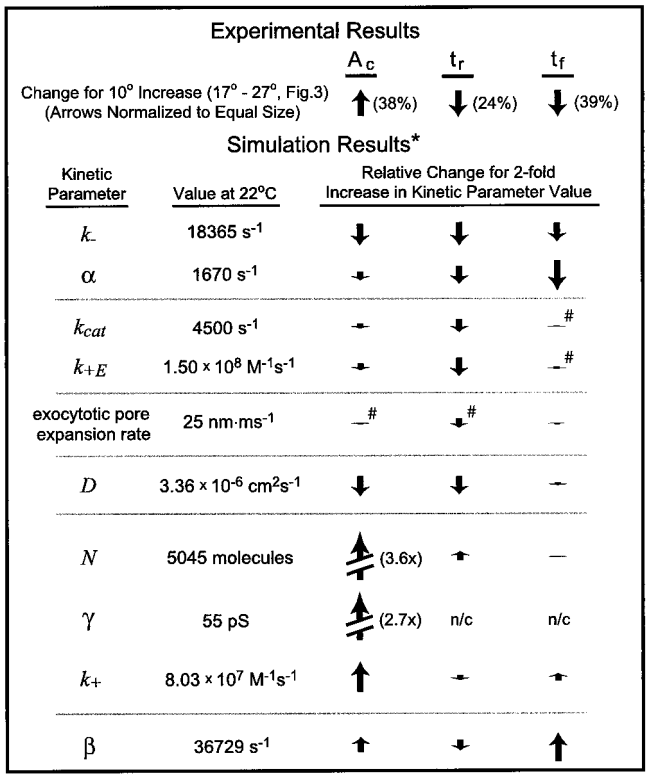

*Size of arrows is normalized to corresponding A_c, t_r, or t_f change shown for Experimental Results (n/c, no change).

#Indicates parameters for which a large decrease in temperature would give a highly asymmetrical response (see Modeling Results and Predictions, and Discussion). Remaining parameters would give approximately equal but opposite changes for decreased rather than increased temperature.

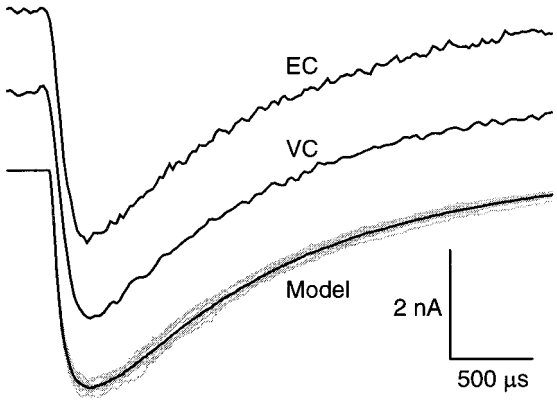

FIGURE 4 Comparison of experimental and model MEPC shape at 22°C. Ten model MEPCs (*thin gray lines*) obtained with different random numbers and the input parameter values of Table 3 are shown together with the corresponding average trace (*thick black line*). Experimental VC and EC curves are averages from 125 MEPCs (3 endplates/animals/recording days) and 86 MEPCs (2 endplates/animals/recording days), respectively. To best illustrate the agreement between mean experimental and model MEPC shapes, individual experimental traces were selected so that: (1) A_c, t_r, and t_f (VC), or t_r and t_f (EC), values were within 75–125% of the mean model values (A_c, 4.12 nA; t_r, 84 μs; t_f, 1.29 ms); (2) the resulting mean experimental values reproduced the mean model values very closely (VC: A_c, 4.14 nA; t_r, 81 μs; t_f, 1.34 ms. EC: t_r, 80 μs; t_f, 1.29 ms). The amplitude of the averaged EC trace was normalized to match that of the VC and model traces.

4 μs, and 1.29 $\pm$ 0.055 ms, respectively. It is possible to use widely different combinations of model input values and reproduce the experimental A_c, t_r, and t_f target values reasonably well, but such other combinations that we have tried are inconsistent with experimental estimates and/or do not simultaneously predict the correct experimental MEPC shape. The final input values used here are all compatible with a variety of earlier experimental and theoretical estimates and, as shown in Fig. 4, closely reproduce the MEPC shape obtained from signal-averaged EC and VC experimental MEPCs.

Predicted temperature dependence of MEPC A_c, t_r, and t_f

From a variety of earlier studies (see Introduction) it appears that some parameters such as k_{cat}, synaptic vesicle fusion pore expansion, and apparent mean channel open time (MBD), have large temperature sensitivities with apparent Q_{10} values of about 3.0. In contrast, D changes only linearly with temperature (from the Einstein relation, $D = RTu$, where R is the gas constant, T is absolute temperature in K, and u is molecular mobility; Schultz, 1980) and thus has a low Q_{10} of about 1.035. The temperature sensitivity of remaining parameters is largely uncertain. Our experimental results from the present study establish that the temperature dependence of MEPC A_c, t_r, and t_f is relatively small, with Q_{10} or $(Q_{10})^{-1}$ values mostly closer to 1.0 than 2.0, and all well below 3.0 (Fig. 3). In the modeling analysis that follows, we determined a minimal model of MEPC temperature sensitivity, and show that changes in two temperature sensitive rates offset each other and account for most of the observed changes in A_c, t_r, and t_f.

Single temperature-sensitive rate model

The simplest possible model of MEPC temperature dependence would include only a single dominant temperature-sensitive rate. We investigated this possibility by varying model parameters individually in computer simulations. Table 3 shows the resulting changes in A_c, t_r, and t_f for a 2-fold increase in each parameter value. The model results are scaled relative to the observed experimental changes in A_c, t_r, and t_f for a 10°C increase centered on 22°C (*middle gray region* in Fig. 3), and in no case do all three model results show the same directions of change that were observed experimentally. Thus, the possibility that a single temperature-sensitive rate dominates the temperature dependence of MEPCs could be ruled out on purely qualitative grounds, indicating that at least two rates must make appreciable contributions.

MEPC t_f: k_- sensitive to temperature

In principle, ten model input parameters (Table 3) taken two at a time yield 45 possible pairs to consider. In practice, however, it was necessary to consider only several combinations because Eq. 2 directly relates t_f to only α, β, and k_-. Table 3 shows that a temperature-dependent change in only α or k_- (i.e., not β) would give the observed direction of change in t_f. However, neither α nor k_- would give the correct change in A_c, and so a minimal model of MEPC temperature dependence requires at least a second parameter paired with either α or k_-, in order to simultaneously produce the observed directions and magnitudes of changes in A_c, t_r, and t_f.

The influence of k_- on A_c strongly outweighs the influence of α (relative lengths of arrows in Table 3) because k_- has a direct impact on the channel opening probability, p_o [from Scheme 1, $p_o = \beta/(\beta + 2k_-)$]. Because changes in p_o can influence the shape of the MEPC peak as well as A_c, we modeled MEPC temperature dependence based on k_- alone to see if the resulting A_c and shape changes would effectively rule out k_- as a dominating temperature-sensitive parameter. With the activation energy (E_a) for k_- assumed to be independent of temperature, the rate constant value was calculated from the Arrhenius equation,

$$k_- = A \cdot e^{-E_a/RT}, \quad (3)$$

where A is the preexponential factor (Barrow, 1981). Keeping all other input parameters fixed at their room temperature values (Table 3), we chose a value for E_a, calculated k_- at several different temperatures, and then ran sets of simulations for those temperatures. We repeated this process until the predicted dependence of t_f on temperature matched the average slope of the experimental curve shown in Fig.

3 *C*. The final value for E_a obtained in this manner was 74.89 kJ mol^{-1}, or 17.90 kcal mol^{-1} ($A = 3.3446 \times 10^{17}\ s^{-1}$).

The apparent Q_{10} values for k_- (ranging from 2.5 to 3.2, Table 4) are reasonable for a biological rate, but nevertheless are 50–90% larger than the corresponding empirical $(Q_{10})^{-1}$ values for experimental t_f (Fig. 3 *C*). Using the E_a value of 74.89 kJ mol^{-1}, we simulated MEPCs over a range of temperatures, and in Fig. 5 the resulting Arrhenius plots for A_c, t_r, and t_f (*open squares*) are compared to the curves (*solid lines*) that we obtained by fitting our experimental data (reproduced from Fig. 3). The simulation results for A_c and t_f are smoothly curved (Fig. 5, *A* and *C*, respectively), while the result for t_r shows a more complex nonlinear shape (Fig. 5 *B*).

Despite the nonlinear Arrhenius plots, the simulation results are not a good reproduction of the experimental results. In particular, the curvature of the simulation t_f data is larger than that for the experimental data (Fig. 5 *C*), the agreement between simulation and experimental t_r results is poor at low temperatures (Fig. 5 *B*), and (most significantly) the simulation curve showing decreased A_c at increased temperature is in pronounced opposition to the experimental curve (Fig. 5 *A*). In addition, Fig. 6 *A* shows that the shape of the simulated MEPCs at low temperatures is not compatible with the corresponding experimental MEPCs, due to an excessive broadening of the peak and early falling phase. These findings for A_c and peak shape rule out k_- as a dominant factor contributing to the MEPC temperature dependence.

Minimal model: α and β sensitive to temperature

With k_- ruled out, α remains as the one parameter that is required to account for decreasing t_f with increasing temperature (Table 3). However, because temperature sensitivity of α alone cannot account for all of our experimental findings, at least one additional temperature-sensitive parameter must be chosen. Temperature sensitivity of β would affect A_c in the required direction and also might reproduce the required curvature for the Arrhenius plot of t_f. A minimal model of MEPC temperature dependence based only on α and β, therefore, has the potential to account for most of the overall A_c, t_r, and t_f changes that occur with changing temperature.

TABLE 4 Apparent Q_{10} values for temperature-sensitive model parameters

Temperature Range (°C)*	k_- Alone	Minimal Model	
		α	β
0–10	3.2	2.7	2.1
17–27	2.8	2.4	1.9
33–43	2.5	2.2	1.8

*The 10° temperature intervals shown are the same as indicated by the shaded regions in Fig 3.

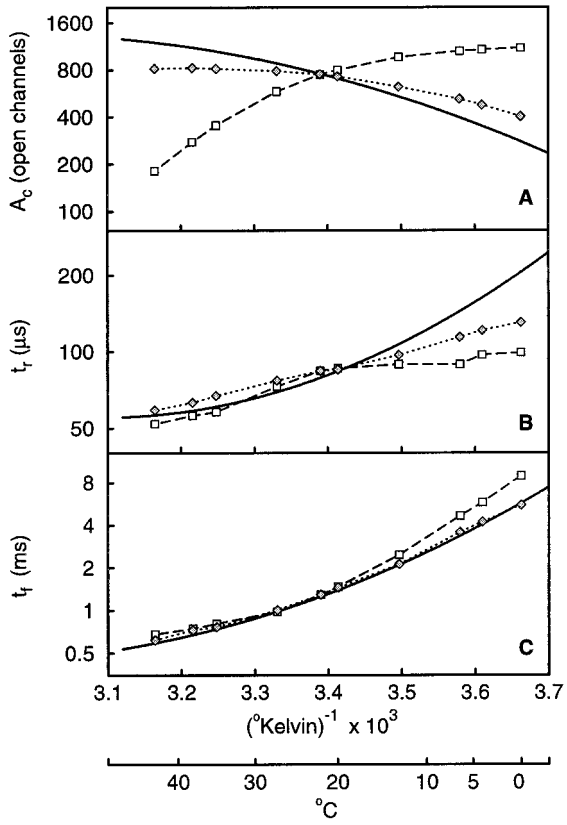

FIGURE 5 Comparison of Arrhenius plots for model and experimental MEPC (*A*) A_c, (*B*) t_r, and (*C*) t_f. Open squares indicate model results obtained when only the rate of ACh unbinding (k_-) was dependent on temperature (based on constant E_a of 74.89 kJ mol^{-1}). Filled diamonds are results obtained with the minimal model of MEPC temperature sensitivity, i.e., with the rates of AChR channel opening and closing (β and α) dependent on temperature (constant E_a values of 46.0 and 63.6 kJ mol^{-1}, respectively). Each model point represents an average value obtained from 10 simulations run with different random numbers, and the range for one SD was smaller than the size of the symbols. Solid lines are the empirical fitting curves obtained from experimental results, and are reproduced from Fig. 3.

In modeling the combined temperature dependence of α and β, we first took the simplest course and assumed that E_a was identical and independent of temperature for the two parameters, making the ratio β/α constant with temperature. As in our modeling based on k_- alone, the only fitting criterion was the average slope of the Arrhenius plot for t_f, compared to the experimental curve shown in Fig. 3 *C* and reproduced in Fig. 5 *C*. We found that the optimal E_a value was similar to that obtained previously for k_-, but that the Arrhenius plot was too highly curved, i.e., t_f was too long at both low and high temperatures (not shown, but similar to the results shown for k_- in Fig. 5 *C*).

To correct the curvature in the Arrhenius plot for t_f, we next allowed α and β to have different but constant E_a values. In this case we searched for the combination of values that reproduced the experimental t_f values measured at the extreme low and high temperatures. For α, the final E_a was 63.6 kJ mol^{-1}, or 15.2 kcal mol^{-1} ($A = 3.043 \times 10^{14}$

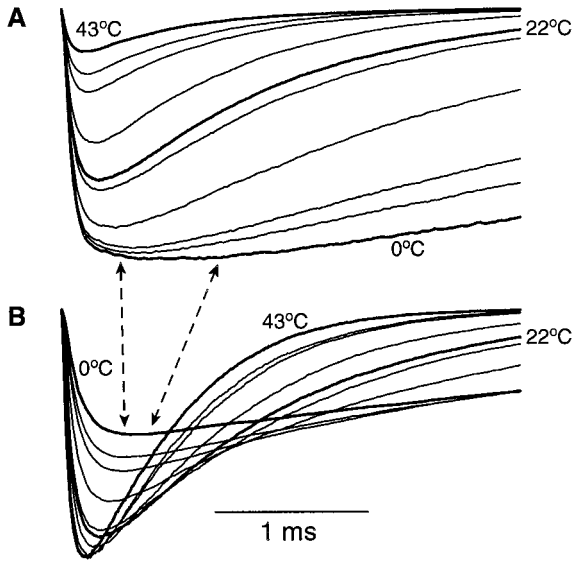

FIGURE 6 Temperature-dependent shape changes for model MEPCs. (*A*) ACh unbinding (k_-) sensitive to temperature. (*B*) AChR gating (α and β) sensitive to temperature. The temperatures for the 10 different curves in each panel correspond to those for the Arrhenius plots of Fig. 5, and each curve is the average obtained from 10 simulations. Dashed arrows indicate excessive broadening of the peak obtained with reduced k_- at low temperatures (*A*), but which was not seen experimentally (Figs. 1 and 2) or with reduced α and β (*B*).

s^{-1}), and for β was 46.0 kJ mol^{-1}, or 11.0 kcal mol^{-1} ($A = 5.177 \times 10^{12}$ s^{-1}). Table 4 shows that the apparent Q_{10} values for α and β ranged from 1.8 to 2.7.

Having determined optimal E_a values for α and β at the extreme high and low temperatures, we then ran simulations for the entire range of temperatures and compared the resulting Arrhenius plots for A_c, t_r, and t_f (Fig. 5, *filled diamonds*) to the corresponding experimental results (*solid curves* reproduced from Fig. 3). As expected, for t_f the simulation and experimental results are essentially indistinguishable. For A_c (Fig. 5 *A*) and t_r (Fig. 5 *B*), the simulation and experimental results are qualitatively similar. Quantitatively, the Arrhenius plot for simulation A_c is smoothly curved like the plot for experimental A_c, but has a slightly shallower overall slope. The plot for simulation t_r is roughly linear and shows good agreement with the experimental t_r data at high temperatures, but at low temperatures the two t_r plots diverge slightly. Figure 6 *B* shows that, with α and β differentially sensitive to temperature, the shape of simulated MEPCs agreed closely with the shape of our experimental MEPCs, and did not show excessive broadening of the peak as amplitude decreased with decreasing temperature. Thus, although our minimal model based on α and β does not exactly reproduce all of our experimental results, it nevertheless shows that the offsetting temperature sensitivities of AChR channel gating mostly govern the temperature dependence of MEPC A_c, t_r, and t_f. Some of the remaining parameters in Table 3 are notable candidates for fine-tuning the model to obtain even closer agreement with experimental data, and such possibilities are presented in the Discussion.

DISCUSSION

Optimized MEPC recordings

Miniature endplate currents are extremely fast signals recorded from very large cells with correspondingly large membrane capacitance and small input resistance. These cellular characteristics represent a large load for a VC circuit, and must be overcome by very large feedback loop gains to achieve fast clamp speeds (loop gain is the multiplication factor applied to the difference between instantaneous membrane potential and the desired holding potential). Unfortunately, large loop gains introduce current measurement problems because stray capacitive currents are enhanced relative to the desired cell membrane current.

Large uncompensated capacitive currents are relatively easy to detect because the measured VC current shows obvious transient overshoot, but small capacitive currents can contribute to what appear as normal MEPCs and can markedly influence the detailed shape of the rising phase and peak. Standard capacitance compensation circuits in commercially available VC amplifiers introduce recording noise (Finkel, 1985), and, with muscle fibers and high loop gains, are generally of little use because MEPCs can be completely obscured by the increased noise. In the present study, we used custom high-speed VC electronics that incorporated variable passive capacitance compensation, so that recording noise was not increased and stray capacitive currents could be critically damped for each pair of recording electrodes in position in the recording bath.

Together with our optimized VC methods, we used EC recording techniques with clearly defined (broad) bandwidth, and electrode tip sizes that minimize t_r artifacts introduced by pressure applied to the endplate while recording (Stiles et al., 1996). We obtained exceedingly close agreement for EC and VC t_r measurements carried out over a very wide range of temperatures (Table 2 and Fig. 3), even up to 43°C where t_r dropped to a minimum of only ~55 μs. We have also recently used these optimized recording methods with frog (*Rana pipiens*) sartorius and cutaneous pectoris muscles, and found that t_r is nearly as fast (~100 μs) as in the lizard (Stiles et al., 1998b), ruling out longer values (200–400 μs) and associated consequences that had been suggested for the time course of ACh exocytosis (see Van der Kloot, 1995). Because of the agreement between our present EC and VC results, we were able to rule out residual current measurement errors arising from either stray capacitances or limited bandwidth. We then could use our results to investigate quantitative models of MEPC temperature dependence based on the activation energy (E_a) of one or more underlying rates.

Modeling the temperature sensitivity of MEPCs

Our modeling results showed that:

1. A nonlinear Arrhenius plot does not necessarily reflect an E_a that itself changes with temperature, as has some-

times been concluded based on the temperature sensitivity of MEPCs (see citations in Introduction). For instance, Fig. 5 shows nonlinear Arrhenius plots obtained for MEPC A_c, t_r, and t_f when only one rate (ACh unbinding, k_-) has a large but constant E_a, or when two rates (AChR channel opening and closing, β and α) have different but constant E_a values.

2. At least two temperature-sensitive rates must contribute to the observed MEPC temperature sensitivity, because changes in any single rate could not simultaneously reproduce the observed directions of change in MEPC A_c, t_r, and t_f (Table 3).
3. A minimal model in which only α and β are sensitive to temperature (E_a values of 63.6 and 46.0 kJ mol^{-1}, respectively, with $E_a = 0$ for all other parameters) reproduced the curved experimental Arrhenius plot for t_f. In this model, the ratio $\beta/2k_- = 1$ at 22°C. A much larger or smaller value of this ratio would reduce or eliminate the curvature of the t_f Arrhenius plot, and hence would degrade agreement with our experimental results. Models where k_- also has a positive E_a (in addition to α and β) could also predict the correct temperature dependence of t_f. From the results shown in Table 3 and Figs. 5 and 6, however, such models would give the correct temperature dependence of MEPC A_c and shape only if the E_a for k_- is appreciably smaller than the E_a values for α and β. Because t_f essentially depends only on α at low temperatures (Eq. 2 simplifies to $1/\alpha$), our model E_a value for α depends little on any other assumptions or parameters. At high temperatures, t_f depends on the ratio $\beta/2k_-$ as well as α (Eq. 2), and therefore our model E_a value for β is a lower limit. The actual E_a for β would be increased by any small non-zero E_a of k_-.
4. The minimal model not only reproduces the experimental temperature dependence of MEPC t_f, but also accounts for much of the observed changes in A_c and t_r (Fig. 5). At low temperatures, both α and β decrease, which prolongs the effective channel gating time (related to $1/(\alpha + \beta)$) and therefore also prolongs t_r. The increased t_r occurs despite a decrease in A_c, which itself stems from a decrease in channel opening probability ($p_o = \beta/(\beta + 2k_-)$). At high temperatures, both A_c and t_r approach asymptotic limits (Fig. 5) because p_o approaches unity and essentially all AChRs open upon reaching the double-bound state. Because t_f approaches $(\beta/\alpha)\cdot 1/2k_-$ at high temperatures (Eq. 2), and because the E_a values for β and α are similar, t_f also changes little at high temperatures.

Fine-tuning the minimal model

To reproduce quantitatively the experimental temperature sensitivity of A_c and t_r, our minimal model would require additional temperature-dependent parameters that slightly increase the sensitivity of A_c across the entire temperature range, and slightly increase the sensitivity of t_r mostly at low temperatures (Fig. 5, *A* and *B*). Because numerous parameters may be involved and may have offsetting effects (Table 3), we cannot suggest a unique, quantitative extension to the minimal model. However, we can suggest several likely possibilities.

A modest temperature sensitivity of nicotinic AChR single-channel conductance (γ) has been reported (Q_{10} values mostly ~1.3, e.g., Sachs and Lecar, 1977; Fishbach and Lass, 1978; Dionne and Parsons, 1981; Hoffman and Dionne, 1983; Dilger et al., 1991). Such changes in γ would increase the temperature sensitivity of A_c without changing either t_r or t_f, and a Q_{10} value of 1.2–1.3 would increase the slope of the model Arrhenius plot for A_c (Fig. 5 *A*) so that it essentially matches our experimental results. Temperature-dependent ACh binding (k_+) would also tend to increase the temperature sensitivity of A_c, and would simultaneously introduce a small effect on t_r in the direction required to fine-tune the minimal model (Table 3). The only remaining parameter in Table 3 that could increase the temperature sensitivity of A_c is N, the average total number of ACh molecules per vesicle. This seems an unlikely factor, however, unless perhaps future studies show that average vesicle volume increases with temperature.

Although many model parameters could conceivably influence the temperature sensitivity of t_r (Table 3), only one seems a likely candidate to prolong t_r mostly at low temperatures. The rate of exocytotic pore expansion appears highly sensitive to temperature (Q_{10} of 3–4, Spruce et al., 1990), and results from Table 3 and our previous simulations of pore expansion (Stiles et al., 1996) show that ACh exocytosis at 22°C and above is rapid enough to produce MEPCs very similar to those obtained with infinitely fast ACh release. However, slower pore expansion at lower temperatures can increase t_r significantly, and also decrease A_c by a smaller factor. Only a 20–50% increase in t_r would be needed to fine-tune the model between 22°C and 0°C (Fig. 5 *B*), so a slowing of pore expansion by only about 10-fold over this temperature range (consistent with a Q_{10} of ~3) might be a significant contributing factor.

Physiological significance of the minimal model

The vertebrate neuromuscular junction must operate as a 1:1 synapse for proper motor coordination, i.e., the multiquantal endplate current must depolarize the muscle beyond threshold each time the nerve fires. To ensure reliable 1:1 transmission, the current is normally much larger than required to reach threshold, and many endplate features contribute to this neuromuscular safety factor (e.g., single axon innervation for nearly synchronous quantal release, maintenance of high postsynaptic AChR density, and tightly coupled pre- and postsynaptic membrane dimensions and structures; Salpeter, 1987; Engel, 1987).

In the present study, we have used highly accurate recordings to show that the temperature sensitivity of MEPCs can be quite small, with apparent Q_{10} values for A_c, t_r, and t_f mostly well below 2 (Fig. 3). Such minimal temperature

sensitivity is of functional benefit to the neuromuscular safety factor and 1:1 transmission, but is perhaps surprising because most biophysical rates show much more pronounced changes with temperature. Our experimental results are qualitatively similar to earlier reports, in which it was sometimes suggested that minimal temperature sensitivity stems from an apparent rate-limiting factor that, itself, shows little change with temperature, e.g., a low Q_{10} for MEPC t_r ascribed to diffusion of ACh in the cleft (Gage and McBurney, 1975). Based on our quantitative Monte Carlo simulations and minimal model, however, we have shown that MEPC temperature sensitivity in fact depends on two dominant underlying rates, AChR channel opening and closing, each of which has a Q_{10} value of at least 2–3 (Table 4). The apparent MEPC temperature sensitivity remains small only because changes in the two rates have opposing rather than synergistic effects.

The authors thank Thomas Bartol, David Colquhoun, and David Deitcher for helpful discussions. Supported by National Institutes of Health K08NS01776 and NSF IBN-9603611 (J.R.S.), Russian Fundamental Research Foundation 96–04-49608 (I.V.K.), and National Institutes of Health NS09315 and GM10422 (M.M.S.).

REFERENCES

Adams, B. A. 1989. Temperature and synaptic efficacy in frog skeletal muscle. *J. Physiol. (Lond.)*. 408:443–455.

Anderson, C. R., and C. F. Stevens. 1973. Voltage clamp analysis of acetylcholine produced end-plate current fluctuations at frog neuromuscular junction. *J. Physiol. (Lond.)*. 235:655–691.

Anglister, L., J. R. Stiles, and M. M. Salpeter. 1994. Acetylcholinesterase density and turnover number at frog neuromuscular junctions, with modeling of their role in synaptic function. *Neuron*. 12:783–794.

Barrow, G. M. 1981. Physical Chemistry for the Life Sciences. McGraw-Hill, New York.

Bartol, T. M., Jr. 1991. A study of miniature endplate current generation at the vertebrate neuromuscular junction using electrophysiology and Monte Carlo simulation. Ph.D. thesis, Cornell University, Ithaca, New York.

Bartol, T. M., B. R. Land, E. E. Salpeter, and M. M. Salpeter. 1991. Monte Carlo simulation of miniature endplate current generation in the vertebrate neuromuscular junction. *Biophys. J.* 59:1290–1307.

Colquhoun, D., and B. Sakmann. 1985. Fast events in single-channel currents activated by acetylcholine and its analogues at the frog muscle end-plate. *J. Physiol. (Lond.)*. 369:501–557.

Dilger, J. P., R. S. Brett, D. M. Poppers, and Y. Liu. 1991. The temperature dependence of some kinetic and conductance properties of acetylcholine receptor channels. *Biochim. Biophys. Acta.* 1063:253–258.

Dionne, V. E., and R. L. Parsons. 1981. Characteristics of the acetylcholine operated channel at twitch and slow fiber neuromuscular junctions of the garter snake. *J. Physiol. (Lond.)*. 310:145–158.

Dwyer, T. M. 1981. The rising phase of the miniature endplate current at the frog neuromuscular junction. *Biochim. Biophys. Acta.* 646:51–60.

Engel, A. G. 1987. The molecular biology of end-plate diseases. *In* The Vertebrate Neuromuscular Junction. M. M. Salpeter, editor. Alan R. Liss, New York. 361–424.

Finkel, A. S. 1985. Useful circuits for voltage clamping with microelectrodes. *In* Voltage and Patch Clamping with Microelectrodes. T. G. Smith, Jr., H. Lecar, S. J. Redman, and P. W. Gage, editors. Williams and Wilkins, Baltimore. 9–24.

Fishbach, G. D., and Y. Lass. 1978. A transition temperature for acetylcholine channel conductance in chick myoballs. *J. Physiol.* 280: 527–536.

Froede, H. C., and I. B. Wilson. 1971. Acetylcholinesterase. *In* The Enzymes, 3rd ed., Vol. 5. P. D. Boyer, editor. Academic Press, New York. 87–114.

Gage, P. W., and R. N. McBurney. 1975. Effects of membrane potential, temperature and neostigmine on the conductance change caused by a quantum of acetylcholine at the toad neuromuscular junction. *J. Physiol. (Lond.)*. 244:385–407.

Harper, A. A., J. R. Shelton, and P. W. Watt. 1989. The temperature dependence of the time course of growth and decay of miniature end-plate currents in carp extraocular muscle following thermal acclimation. *J. Exp. Biol.* 147:237–248.

Head, S. D. 1983. Temperature and end-plate currents in rat diaphragm. *J. Physiol. (Lond.)*. 334:441–459.

Hoffman, H. M., and V. E. Dionne. 1983. Temperature dependence of ion channel permeation at the endplate channel. *J. Gen. Physiol.* 81: 687–703.

Katz, B., and R. Miledi. 1973. The binding of acetylcholine to receptors and its removal from the synaptic cleft. *J. Physiol. (Lond.)*. 231: 549–574.

Kordas, M. 1972. An attempt at an analysis of the factors determining the time course of the end-plate current. II. Temperature. *J. Physiol. (Lond.)*. 224:333–348.

Land, B. R., E. E. Salpeter, and M. M. Salpeter. 1980. Acetylcholine receptor site density affects the rising phase of miniature endplate currents. *Proc. Natl. Acad. Sci. USA.* 77:3736–3740.

Land, B. R., E. E. Salpeter, and M. M. Salpeter. 1981. Kinetic parameters for acetylcholine interaction in intact neuromuscular junction. *Proc. Natl. Acad. Sci. USA.* 78:7200–7204.

Land, B. R., W. V. Harris, E. E. Salpeter, and M. M. Salpeter. 1984. Diffusion and binding constants for acetylcholine derived from the falling phase of miniature endplate currents. *Proc. Natl. Acad. Sci. USA.* 81:1594–1598.

Magleby, K. L., and C. F. Stevens. 1972a. The effect of voltage on the time course of end-plate currents. *J. Physiol. (Lond.)*. 223:151–171.

Magleby, K. L., and C. F. Stevens. 1972b. A quantitative description of end-plate currents. *J. Physiol. (Lond.)*. 223:173–197.

Matthews-Bellinger, J., and M. M. Salpeter. 1978. Distribution of acetylcholine receptors at frog neuromuscular junctions with a discussion of some physiological implications. *J. Physiol. (Lond.)*. 279:197–213.

Robertson, B., and K. T. Wann. 1984. The effect of temperature on the growth and decay times of miniature end-plate currents in the mouse diaphragm. *Brain Res.* 294:346–349.

Rosenberry, T. L. 1975. Acetylcholinesterase. *Adv. Enzymol.* 43:103–208.

Sachs, F., and H. Lecar. 1977. Acetylcholine-induced current fluctuations in tissue-cultured muscle cells under voltage clamp. *Biophys. J.* 17: 129–143.

Salpeter, M. M. 1987. Vertebrate neuromuscular junctions: general morphology, molecular organization, and functional consequences. *In* The Vertebrate Neuromuscular Junction. M. M. Salpeter, editor. Alan R. Liss, New York. 1–54.

Salpeter, M. M., C. D. Smith, and J. A. Matthews-Bellinger. 1984. Acetylcholine receptor at neuromuscular junctions by EM autoradiography using mask analysis and linear sources. *J. Electron Microsc. Tech.* 1:63–81.

Schultz, S. G. 1980. Basic Principles of Membrane Transport. Cambridge University Press, New York.

Spruce, A. E., L. J. Breckenridge, A. K. Lee, and W. Almers. 1990. Properties of the fusion pore that forms during exocytosis of a mast cell secretory granule. *Neuron*. 4:643–654.

Stiles, J. R., T. M. Bartol, H. L. Fernandez, E. E. Salpeter, and M. M. Salpeter. 1992. Neuromuscular communication: inferences from computer simulations of miniature endplate currents. *Soc. Neurosci. Abst.* 18:270.

Stiles, J. R., D. Van Helden, T. M. Bartol, Jr., E. E. Salpeter, and M. M. Salpeter. 1996. Miniature endplate current rise times <100 μs from

improved dual recordings can be modeled with passive acetylcholine diffusion from a synaptic vesicle. *Proc. Natl. Acad. Sci. USA.* 93: 5747–5752.

Stiles, J. R., T. M. Bartol, Jr., E. E. Salpeter, and M. M. Salpeter. 1998a. Monte Carlo simulation of neurotransmitter release using MCell, a general simulator of cellular physiological processes. *In* Computational Neuroscience. J. Bower, editor. Plenum Press, New York. 279–284.

Stiles, J. R., I. Kovyazina, W. Van der Kloot, and M. M. Salpeter. 1998b. Optimized recordings and physiological implications of rapid (~100 μs) miniature endplate current rise times. *Soc. Neurosci. Abst.* 24:826.

Tanzi, F., and E. D'Angelo. 1995. Miniature endplate current kinetics at the mouse neuromuscular junction: effects of temperature and medium viscosity. *Eur. J. Neurosci.* 7:1926–1933.

Tiiska, A. J., and K. Y. H. Lagerspetz. 1994. Thermal acclimation, neuromuscular synaptic delay and miniature end-plate current decay in the frog *Rana temporaria. J. Exp. Biol.* 187:131–142.

Van der Kloot, W. 1995. The rise times of miniature endplate currents suggest that acetylcholine may be released over a period of time. *Biophys. J.* 69:148–154.

Zanello, L. P., E. Aztiria, S. Antollini, and F. J. Barrantes. 1996. Nicotinic acetylcholine receptor channels are influenced by the physical state of their membrane environment. *Biophys. J.* 70:2155–2164.